chemistry

MDPI

Review

The Crystal Chemistry of Inorganic Hydroborates †

Radovan Černý *, Matteo Brighi and Fabrizio Murgia

Laboratory of Crystallography, DQMP, University of Geneva, 24 quai E. Ansermet, CH-1211 Geneva, Switzerland; Matteo.Brighi@unige.ch (M.B.); Fabrizio.Murgia@unige.ch (F.M.)

* Correspondence: Radovan.Cerny@unige.ch

† Dedicated to Dr. Howard Flack (1943–2017).

Academic Editor: Catherine Housecroft

Received: 28 August 2020; Accepted: 23 September 2020; Published: 29 September 2020

Abstract: The crystal structures of inorganic hydroborates (salts and coordination compounds with anions containing hydrogen bonded to boron) except for the simplest anion, borohydride BH_4^-, are analyzed regarding their structural prototypes found in the inorganic databases such as Pearson's Crystal Data [Villars and Cenzual (2015), Pearson's Crystal Data. Crystal Structure Database for Inorganic Compounds, Release 2019/2020, ASM International, Materials Park, Ohio, USA]. Only the compounds with hydroborate as the only type of anion are reviewed, although including compounds gathering more than one different hydroborate (mixed anion). Carbaborane anions and partly halogenated hydroborates are included. Hydroborates containing anions other than hydroborate or neutral molecules such as NH_3 are not discussed. The coordination polyhedra around the cations, including complex cations, and the hydroborate anions are determined and constitute the basis of the structural systematics underlying hydroborates chemistry in various variants of anionic packing. The latter is determined from anion–anion coordination with the help of topology analysis using the program TOPOS [Blatov (2006), IUCr CompComm. Newsl. 7, 4–38]. The Pauling rules for ionic crystals apply only to smaller cations with the observed coordination number within 2–4. For bigger cations, the predictive power of the first Pauling rule is very poor. All non-molecular hydroborate crystal structures can be derived by simple deformation of the close-packed anionic lattices, i.e., cubic close packing (*ccp*) and hexagonal close packing (*hcp*), or body-centered cubic (*bcc*), by filling tetrahedral or octahedral sites. This review on the crystal chemistry of hydroborates is a contribution that should serve as a roadmap for materials engineers to design new materials, synthetic chemists in their search for promising compounds to be prepared, and materials scientists in understanding the properties of novel materials.

Keywords: hydroborate; anions packing; crystal structure

1. Introduction

Hydroborates are anions containing hydrogen bonded to boron. They are also sometimes referred to as "boranes"; this term is, however, used for neutral molecules B_xH_y according to IUPAC [1]. Inorganic hydroborates are salts or coordination compounds where one of the ligands is the hydroborate. The bonding in boron clusters of boranes and hydroborates was explained by Lipscomb [2] using the concept of a three-electron-two-center bond. The concept was further developed in the Polyhedral Skeletal Electron Pair theory (PSEPT) also known as Wade–Mingos rules based on a molecular orbital treatment of the bonding [3,4]. The naming of the boron and hydroborate clusters, used in this review, follows the Wade-Mingos rules: (i) a number of vertices in the polyhedral boron cluster, i.e., dodecaborate for $B_{12}H_{12}^{2-}$ anion, and (ii) the name that describes the topology of the polyhedral cluster, i.e., *closo*-, *nido*- and *arachno*-borates for all polyhedron vertices occupied by boron, and one or two boron atoms missing, respectively.

Inorganic hydroborates were studied as fuels for military applications [5], reducing agents in organic syntheses [6], weakly coordinating anions in catalysis [7,8], for the delivery of ^{10}B for Boron Neutron Capture Therapy (BNCT) [9], as nanocarriers for the delivery of various chemotherapy drugs [10], magnetic resonance imaging (MRI) agents [11], liquid electrolytes [12], and more recently as solid ionic conductors [13,14]. It is exactly the increase of interest in hydroborates as solid-state electrolytes for application in all-solid-state batteries that motivated us to assemble the structural characteristic of known compounds, analyze the coordination of cations and anions, study the type of anion packing, and find the structural aristotypes. The structural systematics discussed in this review attempt to provide a guide to functional inorganic hydroborates design. The hydroborates containing the simplest anion, borohydride BH_4^-, were recently reviewed by us [15] and are not included herein. We will limit our review only to the compounds containing the hydroborate as the only type of anion, although including compounds gathering more than one different hydroborate (mixed anion). We will include in our review also the carbaborane anions where one or more boron atoms are replaced by carbon and partly halogenated hydroborates, i.e., where there is the partial replacement of hydrogen by a halogen. Hydroborates containing anions other than hydroborate or neutral molecules such as NH_3 will not be discussed. Only the compounds in which the crystal structure has been experimentally fully characterized are included; the structures predicted by ab initio calculations or any other method of prediction, but not experimentally confirmed, are excluded. According to our analysis, the crystal chemistry of inorganic large hydroborates is much simpler compared to that of containing small BH_4^- [15] reducing the anion arrangement, for most of the presented compounds, to the packing of hard spheres. We will also show that the first Pauling rule on preferred cation coordination in these (mostly) ionic compounds is limited to small cations, with the coordination number within 2–4 [16].

2. Anions Packing

The hydroborates that form the compounds mostly used in various applications are *closo*-dodecaborates $B_{12}H_{12}^{2-}$ and *closo*-decaborates $B_{10}H_{10}^{2-}$ (Figure 1). While the boron cluster in the first has the form of an ideal icosahedron with the symmetry I_h, the latter is the gyroelongated square bipyramid (bi-capped square antiprism) with the symmetry D_{4d}. The non-crystallographic symmetry of both clusters is at the origin of their orientation disorder in the *ht* phases of many hydroborates.

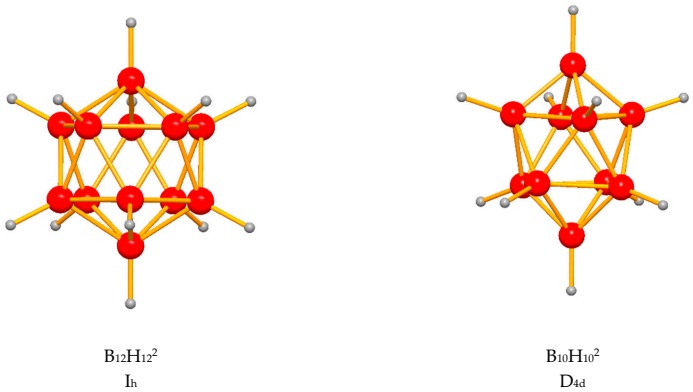

Figure 1. The two frequently used hydroborate anions: *closo*-dodecaborate (**left**) and *closo*-decaborate (**right**) and their point group symmetry.

The high symmetry of the two anions is also responsible for the building principle of corresponding crystal structures based on the packing of hard spheres. Inorganic hydroborates usually contain three types of anion packing: two close packings, cubic close packing (*ccp*) and hexagonal close packing (*hcp*), and one less dense packing in a body-centered cubic cell (*bcc*). However, the poly-anion nature of hydroborates complicates the detections of the packing type, which usually deviates from the ideal packing. For instance, the hexagonal layers of *ccp* or *hcp* are not always parallel to simple crystallographic planes. In some works, the anion packing was analyzed with the algorithms developed for molecular

dynamics (MD) simulation [17], which gives the frequency with which each basic packing maps locally the analyzed structure. This is justified when studying with MD the temporal evolution of some microscopic aspect (such as the distribution of energy barriers for diffusion), and necessarily the atomic positions are given as the atoms' distribution, hence anions packing distribution. However, it makes no sense to use such an algorithm for the analysis of a periodic structure, which gives the averaged description of the structure and where the atoms in the unit cell are located on Wyckoff sites even when the structure is disordered. Instead, the easiest method is to analyze the shape of the first and second coordination sphere of anion–anion interaction, i.e., considering the poly-anions centers: in both close packings, the coordination number of the first sphere is 12, and the polyhedron shape is cuboctahedron for *ccp* (Figure 2a) and anti-cuboctahedron for *hcp* (Figure 2b). In *bcc* packing, the first coordination sphere has a cubic shape, since there are eight nearest neighbors, while the second coordination sphere contains six anions forming an octahedron. Together, the first and second coordination spheres form a rhombic dodecahedron in *bcc* (Figure 2c). We will allocate a type of packing to a given hydroborate, based on the anion–anion coordination polyhedron (which may be deformed) and on the number, type, and connectivity of the interstitial sites, which must not change with respect to the ideal packing.

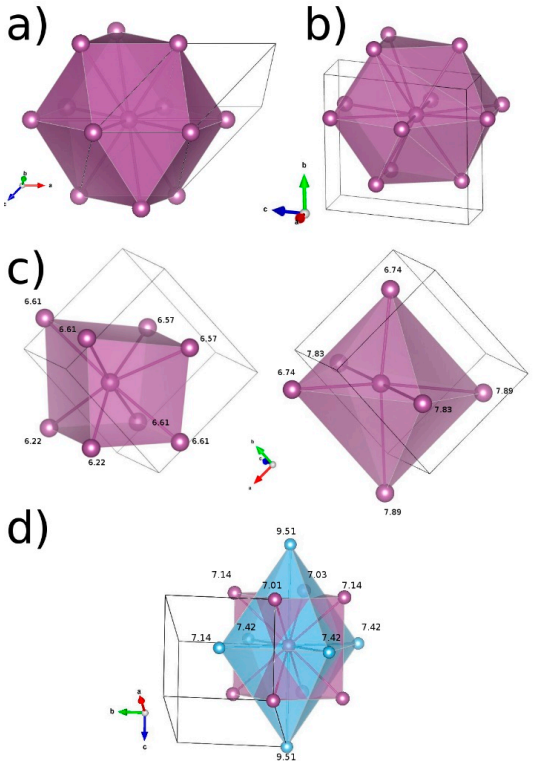

Figure 2. Anion–anion coordination for (**a**) monoclinic *rt*-$Na_2B_{12}H_{12}$ with cubic close packing (*ccp*) of anions. The first coordination sphere contains 12 nearest neighbors at the distance 7.01–7.42 Å forming a cuboctahedron; (**b**) monoclinic *rt*-$K_2B_{10}H_{10}$ with hexagonal close packing (*hcp*) of anions. The first coordination sphere forms an anti-cuboctahedron with a bond distance 6.67–7.68 Å; (**c**) orthorhombic *rt*-$NaCB_9H_{10}$ with body-centered cubic (*bcc*) packing of anions. The first coordination shell is shown on the left, while the second shell is shown on the right (cube and octahedron, respectively). (**d**) Wrong determination of coordination polyhedron for the *rt*-$Na_2B_{12}H_{12}$ leading to the false determination of a *bcc* sublattice. The apical atoms in the octahedron are indeed at the distance of 9.51 Å, while all the others fall in the range 7.0–7.4 Å.

3. Controlling Anions Packing

The type of anion packing is an important parameter controlling hydroborates properties such as cation mobility [18]. While the packing type for monoatomic structures such as metals is simply

driven by space-filling efficiency, it becomes more complex for poly-atomic structures such as ionic compounds. The ability of smaller cations to fill available interstitial sites in the packing of larger anions may control the packing type of the latter [16]. In the case of metal hydroborates, the polyanions are only approximately spherical, and their orientation is controlled by directional metal–hydrogen bonding. It means that in addition to the space-filling and cation/anion size ratio, the cation–anion directional bonding is a third parameter controlling the anion packing [19] at a given temperature and pressure.

Cation distribution on interstitial sites and cation–anion directional bonding are at the basis of the anion packing design and engineering: (1) cation mixing where the larger cation fills the interstitial sites left empty by the smaller (mobile) cation [20,21]; (2) anion mixing, which perturbates the directional cation–anion bonding [22,23], and with the same effect, (3) anion modification such as partial halogenation [21]. In all cases, the volume change and its effect on the total crystal energy cannot be excluded [21].

Anions packing varies also when a neutral molecule such as NH_3 is introduced into the structure of the hydroborate salt [24]. In that case, when the molecule coordinates to the cation, the mobility of the latter is strongly decreased [25].

From the analysis of the anion packing presented here below, it seems that increasing anion anisotropy, i.e., partial halogenation of $B_{12}H_{12}$, use of elongated $B_{10}H_{10}$, or by *carba*-borate and *nido*-borate, increases the probability of having an *hcp* lattice.

4. Preferred Cation Sites

The first Pauling rule predicts the preferred cation coordination in iono-covalent compounds from the ratio of cation and anion radii [16]. We have analyzed all single metal hydroborates presented in this review according to the first Puling rule. The cation radii are according to Shannon [26]. We have used an ionic radius for a given oxidation state contrary to Pauling's original work, which is based on univalent radii. As only very few estimations of hydroborate radii are available in the literature (for BH_4 see [15]), we have used the radii from [27], where the diameter of the anion was calculated as the maximal distance between two terminal hydrogens. Clearly, these radii correspond to the lower limit of the estimation. The calculated cation/anion radius ratios are plotted in Supplementary Materials Figure S1 together with regions corresponding to different cation coordination polyhedra. The agreement of the observed coordination (color of the data point) with the predicted region is relatively good for smaller cations with the observed coordination number within 2–4. For larger cations, the predictive power of the first Pauling rule is very poor, which is in agreement with the recent analysis of Pauling rules validity for oxides [28]. For example, we observe the tetragonal coordination in the region where the octahedral coordination should exist. This discrepancy would be removed if larger anion radii were used, such as estimated from solid crystal structures: 3.18 Å for $B_{10}H_{10}$ [29] or 3.28 Å for $B_{12}H_{12}$ [30] (3.46–3.5 Å from hard spheres approximation) or even larger from the calculation of electrostatic potential surface maps [31]. With larger estimation of the anion size, the predicted region of existence would be shifted to smaller coordination numbers.

5. Anions and Cations Dynamics

The complex anions in the hydroborates can participate in the fast reorientation (rotational) motion. This important dynamical feature contributes to the entropic part of the free energy balance determining thermodynamic stability. Therefore, the information on the anion reorientation dynamics is important for understanding the fundamental properties of hydroborate salts such as the thermal stability and symmetry of the crystal structure. When rotating, the anions approach the spherical symmetry, averaging off the local hydrogen–cation interactions and following more precisely the ideal packing of hard spheres, which leads to stabilizing the higher crystal symmetries in *ht* phases. In addition to the localized reorientation motion of the anions, the long-range motion of the cations is observed in the compounds with high cation conductivity. These two types of atomic motion may be related, i.e., the fast cations diffusion is accompanied by the fast reorientation motion of the

anions [32], as was also shown by ab initio molecular dynamics calculations [33]. The anion and cation dynamics in hydroborates are studied by nuclear magnetic resonance (NMR) [34] and quasi-elastic neutron scattering (QENS) [35]. For more details on the experimental and theoretical studies of the ions dynamics in hydroborates, we refer to the recent review [34].

The ions dynamic is practically invisible in the diffraction experiment using Bragg scattering, which corresponds to the space and time average of atomic positions. The anions reorientation motion and cations long-range diffusion can be only indirectly judged from the observed disorder in atomic positions. If both dynamic and static disorders are present, they may be separated by a temperature-dependent diffraction. The static disorder, if present, persists down to low temperatures where the dynamic one disappears. Some details of the local anion–anion correlation can be obtained by modeling the total scattering (Bragg and diffuse scattering), for example using the Pair Distribution Function analysis. Such experiments have not yet been done on inorganic hydroborates except for salts with a BH_4^- anion [36,37]. The disorder of atomic positions observed from Bragg scattering needs a correct understanding of the superposition of anion point symmetry (Figure 1) with the point symmetry of Wyckoff positions in the crystal. The high non-crystallographic symmetry of the hydroborate anion can fit only partly to a Wyckoff position, and the anion needs to be oriented in such a way that the symmetry elements of a given site match the corresponding symmetry elements of the anions point group. Only in this case do the atomic positions of boron and hydrogen appear fully ordered. If in such ordered structure the anions reorientation happens between orientations that are equivalent by the site symmetry, Bragg scattering cannot detect it. However, if the reorientation occurs between non-equivalent orientations, the structure appears disordered in atomic positions. If this is the case, the Bragg scattering cannot still say whether the disorder is dynamic (i.e., the reorientation of the anion) or whether it is of static nature (i.e., a long-range disorder of anions orientation) [38].

We can demonstrate the interaction between the anions point symmetry and Wyckoff site symmetry on two examples: $Cs_2B_{12}H_{12}$ crystallizes at *rt* in an ordered anti-CaF_2 structure with the crystal symmetry reduced from *Fm*-$\bar{3}$*m* to *Fm*-$\bar{3}$ due to the icosahedral symmetry of the *closo*-anion localized in one orientation (light gray, Figure 3 left). At 529 K, it undergoes a second-order transition of order–disorder type disordering the *closo*-anion by {110} mirror planes (absent in the point symmetry of the anion) increasing the crystal symmetry to *Fm*-$\bar{3}$*m*. Then, the observed disordered anion is a superposition of the anion in two orientations (light and dark gray, Figure 3 right) related by the {110} mirror plane or by the rotation around the anions axis C_3 by 45° (which is equivalent), as shown in Figure 3. This disorder is static as shown by QENS studies where different reorientation jumps about two molecular axes, C_3 by 120° and C_5 by 72°, were suggested [39]. Both jumps exist in *lt* ordered and *ht* disordered phases. They operate independently at a lower temperature, but combine to two-axial jumps at higher temperatures, as shown by ^{1}H and ^{11}B NMR [40].

$Li_2B_{12}H_{12}$ crystallizes at *rt* in an ordered *anti*-CaF_2 structure with its symmetry reduced from *Fm*-3*m* to *Pa*-3 resulting in two *closo*-anions in the unit cell in different orientations but related by the *a*-glide plane (light and dark gray, Figure 3 left). $Li_2B_{12}H_{12}$ undergoes at 628 K a first-order phase transition into the *s.g. Fm*-3*m* where the disordered anion may be explained as a superposition of the two orientations from the *rt*-phase. As the reorientation dynamics in $Li_2B_{12}H_{12}$ has not yet been studied, we cannot conclude whether the disorder in the *ht*-$Li_2B_{12}H_{12}$ is of dynamic or static nature. The phase transition in $Li_2B_{12}H_{12}$ may be compared with that in C60, which crystallizes in an ordered *Pa*-3 structure below 250 K and transforms with first-order order–disorder phase transition connected with the rotation of C60 molecules into an *Fm*-3*m* structure (see Figure S2) [41].

The understanding of cations disorder is easier as there is no interaction between the cations symmetry (single atom) and the symmetry of a Wyckoff site. The observed disorder is always a position disorder, but its nature (dynamic or static) cannot be concluded from Bragg intensities. For example, it is easily identified by measuring the electrical conductivity based on the given cation. As local correlations between moving cations are suggested by molecular dynamic studies [33], the total scattering studies on ionic conductors are of high interest.

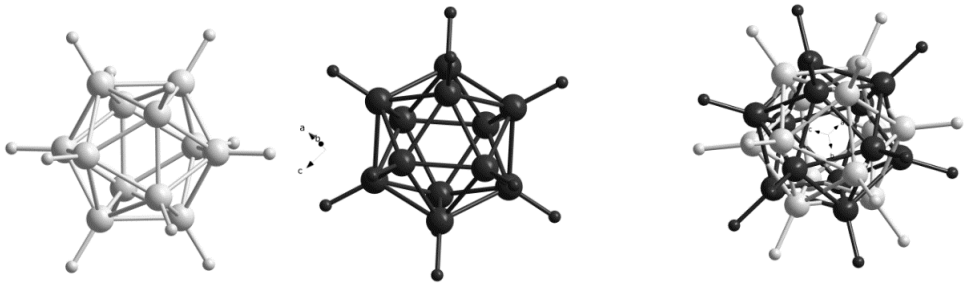

rt-$Li_2B_{12}H_{12}$ and *rt*-$Cs_2B_{12}H_{12}$ *ht*-$Li_2B_{12}H_{12}$ and *ht*-$Cs_2B_{12}H_{12}$

Figure 3. Two orientations, dark and light gray, of the *closo*-anion in the *rt* ordered (s.g. *Pa*-3) and in the *ht* disordered $Li_2B_{12}H_{12}$ (s.g. *Fm*-3) viewed along the C_3 rotation axis of the *closo*-anion. The *rt*-$Cs_2B_{12}H_{12}$ (s.g. *Fm*-3) contains one anion in the orientation identical to the light gray anion in *rt*-$Li_2B_{12}H_{12}$, while the *ht*-$Cs_2B_{12}H_{12}$ (s.g. *Fm*-3*m*) has an identical orientation disorder (rotation around C_3 by 45°) as *ht*-$Li_2B_{12}H_{12}$.

6. Anions Chemistry

According to the aforementioned PSEPT, hydroborates can be thought of as formally made from simple electron donors, i.e., B-H groups, but also C-H in the case of carbaboranes, providing electron density to build up a cluster. The main building block of hydroborates, the B-H unit, accounts for four valence electrons. Excluding the electron pair involved in the boron–hydrogen bond, the remaining two electrons are available to link the boron atoms in non-classical connectivity, where on average two electrons are shared between three boron atoms (three-centers two-electrons). This multicenter interaction is typical of boron-based compounds, due to the intrinsic boron electron deficiency and relatively low electronegativity. As a direct consequence, the possibility of arranging several B-H groups is limited (with fewer exceptions in some open-cage hydroborates [42]), according to 4*n*'s Wade–Mingos rules, to a deltahedron, i.e., a polyhedron with all faces as equilateral triangles. From the point of view of molecular orbitals (MO), each B-H group participates in the formation of three MOs for the cluster bonding, where two are tangent to the cage surface, giving rise to σ superposition of *p* orbitals, while the remaining is oriented inside the cluster and accounts for a further MO. Therefore, *n* B-H building blocks lead to *n*+1 total MOs in the framework. Such non-classical electron distribution implies electron resonance all along the *σ*-bonding in the cage, which, in analogy with carbon chemistry, is often referred to as "superaromaticity". This resonance energy (that accounts for the superior stability of hydroborates compared to other compounds) has been determined for several *closo*-boranes and carba*closo*-boranes up to 12 vertices [43,44]. It is worth noting that the greater the number of B-H units, the higher the stability due to the resonance effect, with a special stabilization shown by 6- and 12-vertex polyhedra. However, in the mono and bi-substituted carba*closo* series, the difference in energy decreases progressively [44], which is likely because the greater electronegativity of the carbon atom(s) withdraws electronic density and limits the resonance along the cage [45]. The progressive removal of one or two boron vertices from a *closo* cage leads to stable open-cage structures, namely *nido*- and *arachno*-boranes. Indeed, retrieving one or two vertices does not change the number of MOs involved in the skeletal binding, since the missing electrons are provided by the addition of hydrogen atoms. However, the loss of quasi-spherical geometry and the consequent reduction of electronic delocalization, besides the more hydridic character of apical hydrogens and their ability to withdraw electrical density from the cage [46], results in the lower chemical stability of the *nido*- and *arachno*-frameworks, with respect to their parent *closo* compounds [47].

7. Classification of Inorganic Hydroborates

Contrary to metal borohydrides [15], the known hydroborates containing larger poly-anions are mostly limited to alkali-metals, alkali-earth, and 3*d* transition metals. No double-cation hydroborate with a large electronegativity difference between the cations is known. Contrary to the borohydrides,

many hydroborate structures with larger hydroborate clusters can be derived not only from a close packed anion lattice (*ccp* or *hcp*) by filling the interstitial tetrahedral (T) and octahedral (O) sites with cations but also from the *bcc* anion packing. The O and T sites are deformed and interpenetrate in *bcc* packing, which makes their occupation by cations less favorable, and neighboring sites cannot be simultaneously occupied. Only very few ionic compounds are based on *bcc* anion packing, contrary to monoatomic structures such as metals. Well-known examples are the *ht* phases of AgI and Ag chalcogenides (S-Te) with Ag_2S being a structural prototype for the *ht* phase of $Na_2B_{12}H_{12}$ (see Figure S2). A common feature of all three *ht* phases, AgI, Ag_2S, and $Na_2B_{12}H_{12}$, is being a superionic conductor with *bcc* anions packing. It is interesting to note that while not a single metal borohydride is based on a *bcc* packing of anions, this anion packing is very often observed among the here-discussed hydroborates with poly-anions, especially at higher temperatures. This is probably a consequence of the weaker cation–hydrogen interaction compared to borohydride, since in hydroborates, the hydridic nature of hydrogen is depleted by the strong electronic density withdrawing toward the boron cage, which is due to the high delocalization among the boron–boron σ bonds in the cage [31,48].

The hydroborates discussed in this review are listed in the following tables: Table 1 contains single cation hydroborates, Table 2 contains double cation hydroborates, and Table 3 contains the hydroborates with inorganic poly-cation. The structural prototypes given in the tables can be found in different crystallographic databases of inorganic compounds such as the Inorganic Crystal Structure Database [49] or Pearson's Crystal Data [50], and in the following, we will not be providing the references for each structural prototype. The occurrence of structural prototypes among the hydroborates is shown in Figure 4, and it is compared with the occurrence among all inorganic compounds as extracted from the Linus Pauling File (LPF) [51].

While the inorganic compounds are dominated by four structure prototypes, NaCl, perovskite, sphalerite, and CsCl, the hydroborates prefer CaF_2, Ni_2In, perovskite (including Ag_3SI), NaCl, and wurtzite (anti-types are included). As already discussed, the prototypes based on anionic *bcc* packing (AgI, Ag_2S, and perovskites) are very common among the hydroborate salts. Other information on the chemistry, synthesis, and application of inorganic hydroborates can be found in recent reviews [15,27,52–58].

The content of the tables is organized in the following way: *First column*: Hydroborates are ordered according to the order of cations in the periodic table. The name describing the topology of the polyhedral cluster is given, too. *Second column*: The symbol of the phase is given as a prefix of the chemical formula only if defined in the original publication. *Third column*: The space group symbol as used in the original publication. If different from the standard setting, the latter is given in parentheses. *Fourth column*: The structural prototype among inorganic compounds. The choice of the prototype is not always in the sense of an *aristotype*, i.e., the most symmetrical structure in the Bärnighausen tree of the given structure (see for example [59]), but rather as a closest structure from which the hydroborate may be derived by replacing anions (i.e., oxides, halides) with hydroborates. The naming of the structural prototypes is according to LPF, i.e., name, Pearson symbol, and space group number [51]. The space group of the prototype or its mineral name is given only if more than one polymorph of the prototype exists. *Fifth column*: Cation coordination. The denticity of the hydroborate coordination, i.e., the number of hydrogen atoms of one hydroborate group coordinating to a given cation, is listed only if the crystal structure was determined by neutron diffraction, single crystal X-ray diffraction, or ab initio solid-state calculations. *Sixth column*: Anion coordination. *Seventh column*: Type of anions packing. If different from three basic packings, the symbol of the anion's net topology is given. The topological analysis was performed with the program TOPOS [60]. The type of molecules packing is given for molecular compounds. The nomenclature used to represent the different nets has been chosen according to the symbolism used in the TOPOS Topological Database (TTD) [61]. *Eighth column*: The given references relate to the most reliable crystal structure determination. If available, one reference for the X-ray and one for the neutron diffraction experiment are given as well as one for the validation of the structure by ab initio solid-state calculations.

Table 1. Structural classification of single cation metal hydroborates.

Cation	Compound	Space Group	Structural Prototype	Cation Coordination by Anions	Cation Coordination by Hydrogen and Halogen	Anion Coordination	Aristotype of Anion Packing	Ref.
Li^+ *closo-*	*rt*-α-$Li_2B_{12}H_{12}$	$Pa\bar{3}$	anti-CaF_2, cF12, 225	Tri-bi	Oct	Oct	*ccp*	[62]
closo-	*ht*-β-$Li_2B_{12}H_{12}$	$Fm\bar{3}$	anti-CaF_2, cF12, 225	Tri			*ccp*	[63,64]
closo-	*rt*-$Li_2B_{10}H_{10}$	$P6_222$	anti-CaF_2, cF12, 225	Tri-bi	Oct	6-fold	$\{3^{36}.4^{46}.5^9\}$ 14-c net; *tcc-x*	[29]
closo-	*ht*-$Li_2B_{10}H_{10}$							[29]
closo-	*rt*-$LiCB_{11}H_{12}$	$Pca2_1$	NaCl, cF8, 225	Tri-bi	Oct	Tri	*ccp*	[65]
closo-	*ht*-$LiCB_{11}H_{12}$	$Fm\bar{3}m$					*ccp*	[65]
closo-	*rt*-α-$LiCB_{11}H_6Cl_6$	*Pnma*	NaCl, cF8, 225	Lin-tri	Oct	NLin	*ccp*	[66]
closo-	*ht*-γ-$LiCB_{11}H_6Cl_6$	$P6_3/mmc$		Lin, Tri			*hcp*	[66]
closo-	*rt*-α-$LiCB_{11}H_6Br_6$	*Pnma*	NaCl, cF8, 225	Lin-tri	Oct	NLin	*ccp*	[66]
closo-	*ht*-γ-$LiCB_{11}H_6Br_6$	$P6_3/mmc$		Lin, Tri			*hcp*	[66]
closo-	*rt*-$LiCB_9H_{10}$							[48]
closo-	*ht1*-$LiCB_9H_{10}$	$Cmc2_1$	wurtzite, hP4, 186				*hcp*	[48]
closo-	*ht2*-$LiCB_9H_{10}$	$P3_1c$	wurtzite, hP4, 186				*hcp*	[48]
nido-	*rt*-$LiB_{11}H_{14}$	*Pbca*	sphalerite, cF8, 216	Tri-mon	Oct	NTri	*ccp*	[67]
nido-	*ht*-$LiB_{11}H_{14}$	$Fm\bar{3}$	sphalerite, cF8, 216	Tri			*ccp*	[67]
closo-	*rt1*-$Li_2(CB_9H_{10})$ $(CB_{11}H_{12})$	$P31c$	wurtzite, hP4, 186				*hcp*	[68]
closo-	*rt2*-$Li_2(CB_9H_{10})$ $(CB_{11}H_{12})$	$Fm\bar{3}m$					*ccp*	[68]
nido, *closo-*	$Li(B_{11}H_{14})_x$ $(CB_{11}H_{12})_{1-x}$ (x = 1/2, 1/3, 2/3)	$Pca2_1$	NaCl, cF8, 225	Tri		Tri	*ccp*	[67]
nido, *closo-*	$Li_{2-x}(B_{11}H_{14})_x(B_{12}H_{12})_{1-x}$ (x = 1/2)	$Pa\bar{3}$	anti-CaF_2, cF12, 225	Tri		Tri	*ccp*	[67]
nido, *closo-*	$Li(B_{11}H_{14})_x$ $(CB_9H_{10})_{1-x}$ (x = 1/2)	$P31c$	wurtzite, hP4, 186	Tet		Tet	*hcp*	[67]
Na^+ *closo-*	*α-rt*-$Na_2B_{12}H_{12}$	$P2_1/n$ ($P2_1/c$)	anti-CaF_2, cF12, 225	Tet-mon, bi, tri	10-fold	Cub	*ccp*	[21,30]
closo-	*β-ht*1-$Na_2B_{12}H_{12}$	$Pm\bar{3}$n	Ag_2S, cI20, 229	Tet			*bcc*	[21,30]
closo-	*γ-ht*2-$Na_2B_{12}H_{12}$	$Im\bar{3}m$	Ag_2S, cI20, 229	Tet			*bcc*	[21,30]
closo-	*δ-ht*3-$Na_2B_{12}H_{12}$	$Fm\bar{3}$	anti-CaF_2, cF12, 225	Tet		Cub	*ccp*	[21]

Table 1. *Cont.*

Cation	Compound	Space Group	Structural Prototype	Cation Coordination by Anions	Cation Coordination by Hydrogen and Halogen	Anion Coordination	Aristotype of Anion Packing	Ref.
closo-	*ε-hp*1-$Na_2B_{12}H_{12}$	*Pbca*	anti-CaF_2, cF12, 225	Tri-bi, tri	7-fold	Oct	*ccp*	[69]
closo-	*ζ-hp*2-$Na_2B_{12}H_{12}$	*Pnnm*	anti-CaF_2, cF12, 225	Tet-mon, bi, tri	9-fold	Cub	*ccp*	[69]
closo-	*m*-$Na_2B_{12}H_{12-x}I_x$	*Pc*	Ni_2In ($Co_{1.75}Ge$), hP6, 194	Tet, Tri		6-fold	*hcp*	[21]
closo-	*h*-$Na_2B_{12}H_{12-x}I_x$	$P6_3mc$	Ni_2In ($Co_{1.75}Ge$), hP6, 194	Tet, Tri		Tet	*hcp*	[21]
closo-	*rt*-$Na_2B_{10}H_{10}$	$P2_1/c$	anti-CaF_2, cF12, 225	Tet-bi, Tet-mon, bi, tri	8-fold, 7-fold	Cub	*ccp*	[70]
closo-	*ht*-$Na_2B_{10}H_{10}$	$Fm\bar{3}m$	anti-CaF_2, cF12, 225	Tet, Oct			*ccp*	[70]
arachno-	NaB_3H_8	$Pmn2_1$	NaCl, cF8, 225	Oct-mon, bi	11-fold	Oct	*ccp*	[71]
closo-	*rt*-$NaCB_{11}H_{12}$	$Pca2_1$	NaCl, cF8, 225	Tri-bi	Oct	Tri	*ccp*	[65]
closo-	*ht*-$NaCB_{11}H_{12}$	$Fm\bar{3}m$					*ccp*	[65]
closo-	*rt*-α-$NaCB_{11}H_6Cl_6$	*Pbca*	sphalerite, cF8, 216	Tri-bi, tri	PentBiPyr	NTri	*ccp*	[66]
closo-	*ht*-γ-$NaCB_{11}H_6Cl_6$	$P6_3/mmc$		Lin, Tri			*hcp*	[66]
closo-	*ht*-γ-$NaCB_{11}H_6Br_6$	$P6_3/mmc$		Lin, Tri			*hcp*	[66]
closo-	*lt*-$NaCB_9H_{10}$	$P2_1/c$	AgI, cI38, 229	Tet-bi	8-fold	Tet	*bcc*	[72]
closo-	*rt*-$NaCB_9H_{10}$	$Pna2_1$	AgI, cI38, 229	Tet-bi	8-fold	Tet	*bcc*	[72]
closo-	*ht*-$NaCB_9H_{10}$	$P3_1c$	wurtzite, hP4, 186				*hcp*	[48]
nido-	*rt*-$NaB_{11}H_{14}$	$Pna2_1$	wurtzite, hP4, 186	Tet, Oct		Tet	*hcp*	[47,73]
nido-	*lt*-$NaB_{11}H_{14}$	$Pna2_1$	wurtzite, hP4, 186	Tet-bi, tri	9-fold	Tet	*hcp*	[47]
nido-	*ht*-$NaB_{11}H_{14}$	$I\bar{4}3d$					*bcc*	[73]
nido-	*rt*-Na-7-$CB_{10}H_{13}$	$Pna2_1$	wurtzite, hP4, 186	Tet-mon, bi, tri	SqAntPris	4-fold	*hcp*	[73]
nido-	*ht*-Na-7-$CB_{10}H_{13}$	$Fm\bar{3}m$					*ccp*	[73]
nido-	*rt*-Na-7,8-$C_2B_9H_{12}$	$P2_1$						[73]
nido-	*ht*-Na-7,8-$C_2B_9H_{12}$	$P31c$					*hcp*	[73]
nido-	*rt*-Na-7,9-$C_2B_9H_{12}$	$Pna2_1$	wurtzite, hP4, 186	Tet-mon, bi, tri	1cap-SqAntPris	4-fold	*hcp*	[73]
nido-	*ht*-Na-7,9-$C_2B_9H_{12}$	$Fm\bar{3}m$					*ccp*	[73]
closo-	$Na_2(B_{12}H_{12})_{0.75}(B_{10}H_{10})_{0.25}$						*bcc*	[74]

Table 1. *Cont.*

Cation	Compound	Space Group	Structural Prototype	Cation Coordination by Anions	Cation Coordination by Hydrogen and Halogen	Anion Coordination	Aristotype of Anion Packing	Ref.
closo-	$Na_2(B_{12}H_{12})_{0.50}(B_{10}H_{10})_{0.50}$	$Fm\bar{3}m$	anti-CaF_2, cF12, 225	Tet, Oct			*ccp*	[75]
closo-	*rt*-$Na_{2-x}(CB_{11}H_{12})_x(B_{12}H_{12})_{1-x}$ (x = 1/2, 1/3, 2/3)	$I23$	Ag_3SI, (anti-perovskite) cP5, 221	Tet			*bcc*	[22]
closo-	*ht1*-$Na_{2-x}(CB_{11}H_{12})_x(B_{12}H_{12})_{1-x}$ (x = 1/3)	$Pm\bar{3}n$	Ag_3SI, (anti-perovskite) cP5, 221	Tet			*bcc*	[22]
closo-	*ht2*-$Na_{2-x}(CB_{11}H_{12})_x(B_{12}H_{12})_{1-x}$ (x = 1/3)	$Im\bar{3}m$	Ag_3SI, (anti-perovskite) cP5, 221	Tet			*bcc*	[22]
closo-	$Na_3(CB_9H_{10})$ $(B_{12}H_{12})$	$P\bar{4}2_1c$	Ag_3SI, (anti-perovskite) cP5, 221	Tet			*bcc*	[18]
closo-	$Na_3(CB_{11}H_{12})$ $(B_{10}H_{10})$	$Pnnm$	anti-CaF_2, cF12, 225	Tet, Tri			*ccp*	[18]
closo-	*rt1*-$Na_2(CB_9H_{10})$ $(CB_{11}H_{12})$	$P3_1c$	wurtzite, hP4, 186	Tri			*hcp*	[18,68]
closo-	*rt2*-$Na_2(CB_9H_{10})$ $(CB_{11}H_{12})$	$Fm\bar{3}m$					*ccp*	[68]
nido, closo-	$Na_{2-x}(B_{11}H_{14})_x(B_{12}H_{12})_{1-x}$ (x = 1/2, 2/3)	$Im\bar{3}m$	Ag_3SI, (anti-perovskite) cP5, 221	Tet			*bcc*	[47]
nido, closo-	*rt*-$Na_{2-x}(B_{11}H_{14})_x(B_{12}H_{12})_{1-x}$ (x = 1/3)	$Pm\bar{3}n$	Ag_3SI, (anti-perovskite) cP5, 221	Tet			*bcc*	[47]
nido, closo-	*ht*-$Na_{2-x}(B_{11}H_{14})_x(B_{12}H_{12})_{1-x}$ (x = 1/3)	$Im\bar{3}m$	Ag_3SI, (anti-perovskite) cP5, 221	Tet			*bcc*	[47]
nido, closo-	$Na_3BH_4B_{12}H_{12}$	$Cmc2_1$	novel	Tet			*CrB*	[23]
K^+ *closo-*	$K_2B_{12}H_{12}$	$Fm\bar{3}$	anti-CaF_2, cF12, 225	Tet-tri	Cuboct	Cub	*ccp*	[76]
closo-	$K_2B_{10}H_{10}$	$P2_1/c$	Ni_2In ($Co_{1.75}Ge$), hP6, 194	Tet-tri, Oct-mon, bi, tri, tetra	12-fold, 14-fold	2cap-SqAntPris	*hcp*	[77]
arachno-	α-KB_3H_8	$P2_1/m$	NaCl, cF8, 225	Oct-tri, tetra, penta	24-fold	Oct	*ccp*	[78]
arachno-	α′-KB_3H_8	$Cmcm$	NaCl, cF8, 225	Oct-bi, tri, tetra	18-fold	Oct	*ccp*	[78]
arachno-	β-KB_3H_8	$Fm\bar{3}m$	NaCl, cF8, 225	Oct		Oct	*ccp*	[78]
closo-	$K_2B_6H_6$	$Fm\bar{3}m$	anti-CaF_2, cF12, 225	Tet-tri	Cuboct	Cub	*ccp*	[79]
closo-	*rt*-$KCB_{11}H_{12}$	$P2_1/c$	NaCl, cF8, 225	Oct-mon, bi, tri	12-fold, 10-fold	Oct	*ccp*	[80]
closo-	*ht*-$KCB_{11}H_{12}$	$Fm\bar{3}m$	NaCl, cF8, 225	Oct		Oct	*ccp*	[80]

Table 1. *Cont.*

Cation	Compound	Space Group	Structural Prototype	Cation Coordination by Anions	Cation Coordination by Hydrogen and Halogen	Anion Coordination	Aristotype of Anion Packing	Ref.
closo, closo-	$KB_{21}H_{18}$	*C*2	NiAs, hP4, 194	TriAntPris-mon, tri	14-fold	TriPris	*hcp*	[81]
nido, closo-	*m*-$K_3BH_4B_{12}H_{12}$	*P*2/*c*	Ag_3SI, (anti-perovskite) cP5, 221	Oct-bi, tri	14-fold	BH_4-Oct, $B_{12}H_{12}$-Cuboct	*bcc*	[82]
nido, closo-	*r*-$K_3BH_4B_{12}H_{12}$	$R\bar{3}m$	Ag_3SI, (anti-perovskite) cP5, 221	Oct		BH_4-Oct, $B_{12}H_{12}$-Cuboct	*bcc*	[82]
nido, closo-	*c*-$K_3BH_4B_{12}H_{12}$	*P*23	Ag_3SI, (anti-perovskite) cP5, 221	Oct		BH_4-Oct, $B_{12}H_{12}$-Cuboct	*bcc*	[82]
Rb+ *closo-*	$Rb_2B_{12}H_{12}$	$Fm\bar{3}$	anti-CaF_2, cF12, 225	Tet-tri	Cuboct	Cub	*ccp*	[83]
closo-	*rt*-$Rb_2B_{10}H_{10}$	$P2_1/c$	Ni_2In ($Co_{1.75}Ge$), hP6, 194	Tet-bi, tri, tetra Oct-mon, bi, tri, tetra	12-fold, 17-fold	3cap-SqAntPris	*hcp*	[77,84]
closo-	*lt*-$Rb_2B_{10}H_{10}$	$P\bar{1}$	Ni_2In ($Co_{1.75}Ge$), hP6, 194	Tet-bi, tri, tetra Oct-mon, bi, tri, tetra	12-fold, 17-fold	3cap-SqAntPris	*hcp*	[84]
closo-	$Rb_2B_9H_9$	*P*4/*nmm*	anti-BiF_3, cF16, 225	Tet-tri, SqPyr-bi, tri	Cuboct, 14-fold	4cap-TriPris	*ccp*	[85]
closo, closo-	$Rb_2B_{20}H_{18}$	$Pna2_1$	anti-$MoSi_2$, tI6, 139	SqPyr-mon, tri	13-fold	2cap-Cub	Mo in $MoSi_2$ $\{3^{48}.4^{66}.5^6\}$ 16-c net	[86]
nido, closo-	$Rb_3BH_4B_{12}H_{12}$	*P*23	Ag_3SI, (anti-perovskite) cP5, 221	Oct		BH_4-Oct, $B_{12}H_{12}$-Cuboct	*bcc*	[87]
Cs^+ *closo-*	*rt*-$Cs_2B_{12}H_{12}$	$Fm\bar{3}$	anti-CaF_2, cF12, 225	Tet-tri	Cuboct	Cub	*ccp*	[88]
closo-	*ht*-$Cs_2B_{12}H_{12}$	$Fm\bar{3}m$	anti-CaF_2, cF12, 225	Tet		Cub	*ccp*	[89]
closo-	$Cs_2B_6H_6$	$Fm\bar{3}m$	anti-CaF_2, cF12, 225	Tet-tri	Cuboct	Cub	*ccp*	[90]
arachno-	CsB_3H_8	*Ama*2	NaCl, cF8, 225	Oct-bi, tri, tetra	16-fold	Oct	*ccp*	[90]
closo-	$Cs_2B_8H_8$	*Pnma*	Ni_2In ($Co_{1.75}Ge$), hP6, 194	Tet-tri, SqPyr-bi, tri	12-fold	1cap-SqAntPris	*hcp*	[91]
nido-	CsB_9H_{14}	$P\bar{1}$	CsCl, cP2, 221	Cub		Cub	*aa*	[92]
closo, closo-	$CsB_{21}H_{18}$	$P2_1/c$	NaCl, cF8, 225	TriAntPris-mon, bi, tri	15-fold	TriAntPris	*ccp*	[93]
closo-	*rt*-$CsCB_{11}H_{12}$	*R*3 (*R*3/*c* above 323 K)	novel	Oct-bi, tri	15-fold	6-fold	*hcp*	[94]

Table 1. *Cont.*

Cation	Compound	Space Group	Structural Prototype	Cation Coordination by Anions	Cation Coordination by Hydrogen and Halogen	Anion Coordination	Aristotype of Anion Packing	Ref.
closo-	*ht*-$CsCB_{11}H_{12}$	$I\bar{4}3d$	Th_3P_4, cI28, 220	Oct-bi, tri	14-fold	8-fold	*hcp*	[94]
closo-	$CsCB_{11}H_6Cl_6$	$P2/c$	CsCl, cP2, 221	Cub-bi, tri	6cap-Cub, 16-fold	Cub	*aa*	[95]
closo-	$CsCB_{11}H_{11}Br_1$	$P2_1/n$	NaCl, cF8, 225	Oct-mon, bi, tri	12-fold	Oct	*ccp*	[96]
closo-	$CsCB_{11}H_6Br_6$	$P2/c$	CsCl, cP2, 221	Cub-bi, tri	6cap-Cub, 16-fold	Cub	*aa*	[95]
closo-	$CsCB_9H_5Br_5$	$P4/nmm$	sphalerite, cF8, 216	Tet-tri	Cuboct	Tet	*ccp*	[95]
nido-	α-$CsC_2B_9H_{12}$	$I4$	AgI, cI38, 229	Tet		SqPris	*bcc*	[97]
nido-	β-$CsC_2B_9H_{12}$	$P2_1/c$	NiAs, hP4, 194—CsCl, cP2, 221	8-fold		8-fold	*hcp*	[97]
nido-	γ-$CsC_2B_9H_{12}$	$P2_1/c$	NiAs, hP4, 194	Oct		TriPris	*hcp*	[97]
closo, *closo-*	$Cs(B_{21}H_{18-x}F_x)$ (x = 2.55–2.85)	$P2_1/n$ ($P2_1/c$)	NiAs, hP4, 194	TriAntPris-bi, tri, tetra	18-fold	TriPris	*hcp*	[93]
closo, *closo-*	$Cs(B_{21}H_{18-x}F_x)$ (x = 2.85–3)	$P2_12_12_1$	NiAs, hP4, 194	TriAntPris-bi, tri, tetra	18-fold	TriPris	*hcp*	[93]
nido, *closo-*	$Cs_3BH_4B_{12}H_{12}$	$P23$	Ag_3SI, (anti-perovskite) cP5, 221	Oct-bi	Cuboct	BH_4-Oct, $B_{12}H_{12}$-Cuboct	*bcc*	[98]
Be^{2+} *arachno-*	$Be(B_3H_8)_2$	$P2_1/c$		Lin-bi	Tet		*ccp* of $Be(B_3H_8)_2$ molecules	[99]
arachno- *nido-*	$Be(B_5H_{10})BH_4$	$P2_1/c$		Lin-bi	Tet		*ccp* of $Be(B_5H_{10})BH_4$ molecules	[100]
Ca^{2+} *closo-*	$CaB_{12}H_{12}$	$C2/c$	BN-b, hP4, 194	TriBiPyr-mon, bi	8-fold	TriBiPyr	*hcp*	[101]
closo-	α-$CaB_{10}H_{10}$	Cc	wurtzite, hP4, 186	Tet-mon, tri	10-fold	Tet	*hcp*	[102]
closo-	β-$CaB_{10}H_{10}$	$Pbca$	$FePO_4$, oP48, 61	Tet-bi, tri	10-fold	Tet	*hcp*	[102]
Sr^{2+} *closo-*	$SrB_{12}H_{12}$	$P31c$	wurtzite, hP4, 186	Tet-tri	Cuboct	Tet	*hcp*	[103]

Table 1. *Cont.*

Cation	Compound	Space Group	Structural Prototype	Cation Coordination by Anions	Cation Coordination by Hydrogen and Halogen	Anion Coordination	Aristotype of Anion Packing	Ref.
Ba^{2+} *closo-*	$BaB_{12}H_{12}$	*P*31*c*	wurtzite, hP4, 186	Tet-tri	Cuboct	Tet	*hcp*	[103]
Cr^{2+} *arachno-*	$Cr(B_3H_8)_2$	$P\bar{1}$		Lin-bi	Sq		*aa* of $Cr(B_3H_8)_2$ molecules	[104]
Mn^{2+} *closo-*	$MnB_{12}H_{12}$	*P*31*c*	BN-b, hP4, 194	Lin-tri	Oct	Lin	*hcp*	[105]
Fe^{2+} *closo-*	$FeB_{12}H_{12}$	$R\bar{3}$		Lin-tri	Oct	Tri	*bcc*	[105]
Co^{2+} *closo-*	$CoB_{12}H_{12}$	$R\bar{3}$		Lin-tri	Oct	Tri	*bcc*	[106]
Ni^{2+} *closo-*	$NiB_{12}H_{12}$	$R\bar{3}$		Lin-tri	Oct	Tri	*bcc*	[106,107]
Cu^{+} *closo-*	$Cu_2B_{12}H_{12}$	$Pn\bar{3}$	Cu_2O, cP6, 224	Lin-bi	4-fold	Tet	*bcc*	[106]
Ag^{+} *closo-*	α-$Ag_2B_{12}H_{12}$	$Pa\bar{3}$	anti-CaF_2, cF12, 225	Tri-bi	TriAntPris	TriAntPris	*ccp*	[108]
closo-	β-$Ag_2B_{12}H_{12}$	$Fm\bar{3}m$	anti-CaF_2, cF12, 225	Tet		Cub	*ccp*	[108]
closo-	α-$Ag_2B_{10}H_{10}$	*P*4/*nnc*	anti-CaF_2, cF12, 225	Tet-tri	Cuboct	Cub	*ccp*	[108]
closo-	β-$Ag_2B_{10}H_{10}$	$Fm\bar{3}m$	anti-CaF_2, cF12, 225	Tet		Cub	*ccp*	[108]
closo-	$AgCB_9H_{10}$	$P2_1/m$	NaCl, cF8, 225	TriAntPris-mon, tri	10-fold	TriPris	*ccp*	[109]
closo-	$AgCB_{11}H_6Br_6$	*Pnma*	NaCl, cF8, 225	Lin-tri	Oct	NLin	*ccp*	[110]
Hg^{2+} *closo-*	$HgB_{12}H_{12}$	$P\bar{1}$	CsCl, cP2, 221	Cub		Cub	*ccp*	[111]
Tl^{+} *closo-*	$Tl_2B_{10}H_{10}$	$Fm\bar{3}$	anti-CaF_2, cF12, 225	Tet-tri	Cuboct	Cub	*ccp*	[112]
Pb^{2+} *closo-*	$PbB_{12}H_{12}$	*P*31*c*	wurtzite, hP4, 186	Tet-tri	Cuboct	Tet	*hcp*	[113]

Abbreviations: Term = terminal, Lin = collinear, NLin = non-collinear, Tri = coplanar triangular, NTri = non-coplanar triangular, Sq = square, Sad = saddle-like, Tet = tetrahedron or tetragonal, Pent = pentagonal, Oct = octahedron, Hex = hexagonal, Rho = rhombic, Cuboct = cuboctahedron, Dodeca = dodecahedron, Pris = prism, Pyr = pyramid, Ant = anti, cap = capped. The degree of deformation of the coordination polyhedron from ideal shape is not specified. mon = monodentate, bi = bidentate, tri = tridentate. *lt* = low temperature, *rt* = room temperature, *ht* = high temperature, *hp* = high pressure, *m* = monoclinic, *o* = orthorhombic, *h* = hexagonal (refers to different polymorphs). *ccp* = cubic close packed, *hcp* = hexagonal close packed, *bcc* = body-centered cubic, *aa* = simple sequence of hexagonal layers. 1: gyroelongated square bipyramid; 2: triangular orthobicupola; 3: snub disphenoid (dodecadeltahedron). Color coding: alkali metals: brown; alkali earth metals: orange; rare earths: magenta; transition elements: blue; actinides: dark green; other metals: light green.

Table 2. Structural classification of double cation metal hydroborates. See the caption of Table 1 for details.

Cation	Compound	Space Group	Structural Prototype	Cation Coordination by Anions	Cation Coordination by Hydrogen	Anion Coordination	Anion Packing	Ref.
Li^+, Na^+ *closo-*	*rt*-$(Li_x,Na_{1-x})_2B_{12}H_{12}$ (x = 0.33–0.67)	$Pa\bar{3}$	anti-CaF_2, cF12, 225	Tri-bi	Oct	Oct	*ccp*	[114]
closo-	*ht*-$(Li_x,Na_{1-x})_2B_{12}H_{12}$ (x = 0.377)	$Fm\bar{3}m$	anti-CaF_2, cF12, 225	Tri			*ccp*	[115]
nido-, *closo-*	$(Li_{0.7}Na_{0.3})_3BH_4B_{12}H_{12}$	$Pna2_1$	novel	Tet			*FeB*	[23]
Li^+, K^+ *closo-*	*rt*-$LiKB_{12}H_{12}$	$P6_3mc$	Ni_2In ($Co_{1.75}Ge$), hP6, 194	Li-Tri-bi, K-Oct-bi, tri	Li-TriPris K-15-fold	3cap-TriPris	*hcp*	[116]
closo-	*ht*-$(Li_x,K_{1-x})_2B_{12}H_{12}$ (x = 0.8)	$P6_3mc$	Ni_2In ($Co_{1.75}Ge$), hP6, 194	Li-Tri, (K,Li)-Oct		3cap-TriPris	*hcp*	[21]
Li^+, Cs^+ *closo-*	*rt*-$LiCsB_{12}H_{12}$	$Pn2_1a$	Ni_2In ($Co_{1.75}Ge$), hP6, 194	Li-Tri, Cs-Oct		3cap-TriPris	*hcp*	[21]
closo-	*ht*-$LiCsB_{12}H_{12}$	$P6_3mc$	Ni_2In ($Co_{1.75}Ge$), hP6, 194	Li-Tri, Cs-Oct		3cap-TriPris	*hcp*	[21]
closo-	*meta*-$(Li_x,Cs_{1-x})_2B_{12}H_{12}$ (x = 0.11)	$P6_3mc$	Ni_2In ($Co_{1.75}Ge$), hP6, 194	(Cs,Li)-Tri, Tet Cs-Oct		10-fold	*hcp*	[21]
Na^+, K^+ *closo-*	*rt*-$(Na_x,K_{1-x})_2B_{12}H_{12}$ (x = 0.5)	$Fm\bar{3}$	anti-CaF_2, cF12, 225	Tet-tri	Cuboct	Cub	*ccp*	[21]
closo-	*ht*-$(Na_x,K_{1-x})_2B_{12}H_{12}$ (x = 0.5)	$Pm\bar{3}n$	Ag_2S, cI20, 229	Tet			*bcc*	[21]
closo-	*rt*-$NaKB_{12}H_{12}$	$P1$	Ni_2In ($Co_{1.75}Ge$), hP6, 194	Na-Tet, K-Oct		4cap-TriPris	*hcp*	[21]
closo-	*ht*-$NaKB_{12}H_{12}$	$P6_3mc$	Ni_2In ($Co_{1.75}Ge$), hP6, 194	Na-Tet, K-Oct		4cap-TriPris	*hcp*	[21]
Na^+, Cs^+ *closo-*	*rt*-$NaCsB_{12}H_{12}$	$P\bar{1}$	Ni_2In ($Co_{1.75}Ge$), hP6, 194	Na-Tet, Cs-Oct		4cap-TriPris	*hcp*	[21]
closo-	*ht1*-$NaCsB_{12}H_{12}$	$P2_1/c$	Ni_2In ($Co_{1.75}Ge$), hP6, 194	Na-Tet, Cs-Oct		4cap-TriPris	*hcp*	[21]
closo-	*ht2*-$NaCsB_{12}H_{12}$	$Pn2_1a$	Ni_2In ($Co_{1.75}Ge$), hP6, 194	Na-Tet, Cs-Oct		4cap-TriPris	*hcp*	[21]
closo-	*ht3*-$NaCsB_{12}H_{12}$	$P6_3mc$	Ni_2In ($Co_{1.75}Ge$), hP6, 194	Na-Tet, Cs-Oct		4cap-TriPris	*hcp*	[21]
Cs^+,Cu^+ *closo-*	$Cs(CuB_{10}H_{10})$	*Pbcn*	novel	Cs- Oct-mon, bi, tri Cu-Lin-bi	Cs-15-fold Cu-Tet	8-fold	*ccp*	[117]
Cs^+,Ag^+ *closo-*	$Cs(AgB_{10}H_{10})$	*Pbcm*	anti-BiF_3, cF16, 225	Cs-Oct-mon, bi, tri Ag-Tet-bi	Cs-15-fold Ag-8-fold	2cap-SqAntPris	*ccp*	[118]

Color coding: alkali metals: brown; transition elements: blue.

Table 3. Structural classification of hydroborates with complex inorganic cations. See the caption of Table 1 for details.

Cation	Compound	Space Group	Structural Prototype	Cation Coordination by Anions	Cation Coordination by Hydrogen	Anion Coordination	Anion Packing	Ref.
NH_4^+ *closo-*	$(NH_4)_2B_{12}H_{12}$	$Fm\bar{3}$	anti-CaF_2, cF12, 225	Tet-tri	Cuboct	Cub	*ccp*	[83]
closo-	$(NH_4)_2B_{10}H_{10}$	$P2_1/c$	Ni_2In ($Co_{1.75}Ge$), hP6, 194	Tet, Oct		8-fold	*hcp*	[119]
arachno-	$NH_4B_3H_8$	*Cmcm*	NaCl, cF8, 225	Oct-bi, tri, tetra	18-fold	Oct	*ccp*	[120]
$N_2H_5^+$ *closo-*	$(N_2H_5)_2B_{12}H_{12}$	*C*2/*c*	anti-AlB_2, hP3, 191	TriPris		HexPris	*aa*	[121]
$N(n\text{-}Bu_4)^+$ *closo-*	$N(n\text{-}Bu_4)B_8H_9$	$P4_1$	LiSe subnet in NH_4LiSeO_4, oP28, 33	Tet		Sq	*aa*	[91]
closo-	$N(n\text{-}Bu_4)_2B_7H_7$	$P2_1/n$ ($P2_1/c$)	anti-NiP subnet in $Ba_2Ni(PO_4)_2$, mP52, 14	Tri, Lin		TriBiPyr	*hcp*	[122]
closo-	$N(n\text{-}Bu_4)B_7H_8$	$P4_1$	LiSe subnet in NH_4LiSeO_4, oP28, 33	Sq		Sq	*aa*	[122]
Ph_4P^+ *closo-*	lt-$(Ph_4P)B_8H_9$	*P*2/*c*	CsCl, cP2, 221	SqAntPris		Cub	*aa*	[91]
closo-	rt-$(Ph_4P)B_8H_9$	*P*4/*n*	CsCl, cP2, 221	SqAntPris		Cub	*aa*	[91]
Ph_3P^+ *nido-*	$(Ph_3P)B_{11}H_{14}$	$P2_1/m$	BN-b, hP4, 194	TriBiPyr		TriBiPyr	*aa*	[123]
PNP^+ *closo-*	$(PNP)B_7H_8$	$P2_1/c$	novel	9-fold		9-fold	*aa*	[122]
$HAgu^+$ *closo-*	$(HAgu)_2B_{12}H_{12}$	$P\bar{1}$	anti-AlB_2, hP3, 191	TriPris		HexPris	*aa*	[124]
$HAgu^+$ Cu^{2+} *closo-*	$(Cu_{0.61}H_{0.78}Agu_2)B_{12}H_{12}$	$P\bar{1}$	CsCl, cP2, 221	RhoPris		RhoPris	*aa*	[124]

Color coding: transition elements: blue.

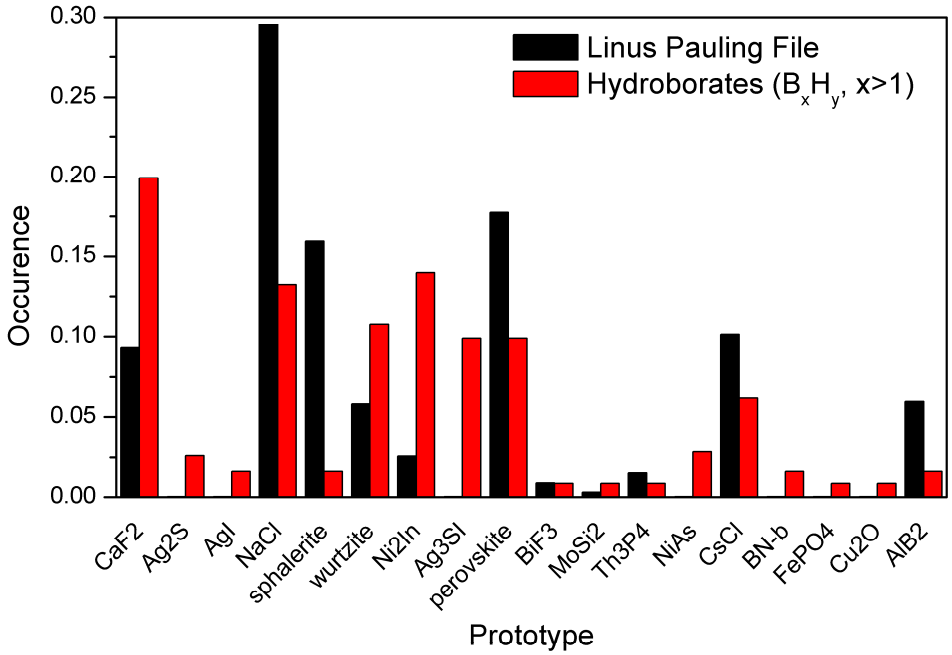

Figure 4. Occurrence of selected structural prototypes among binary inorganic compounds extracted from the Linus Pauling File [51], and among the hydroborates (excluding borohydrides with BH_4^- anion). Both graphs include ternary solid solutions. The fractions are renormalized, to sum up to one for each graph.

8. Conclusions

Contrary to borohydrides, where all types of inorganic solid compounds can be found ranging from salts based on anions packing up to 2D and 3D coordination polymers, the higher hydroborates usually form salts where the large hydroborate anions pack, in most cases, according to one of the three common packings. The exception are hydroborates of Be that form molecular compounds, and transition metals hydroborates, which have still a packed anion sublattice, but the resulting metal–anion interaction is covalent, classifying these compounds as coordination polymers. The same is valid also for double cation hydroborates, while the situation is different for poly-cations, where the compact anion sublattice is broken as a consequence of the directional anion–cation bonds. The exception is the nearly spherical (if orientationally disordered) NH_4^+ cation.

Contrary to other inorganic compounds, the hydroborate salts crystallize very often with the *bcc* anion packing, favoring 3D pathways based on tetrahedral sites for high cation mobility. The anion packing can be best controlled by anion mixing and to a certain extend by anion modification. The mixing of cations and inclusion of neutral molecules in the crystal has a negative effect on cations mobility. The knowledge of anions packing and the ability to control it play an important role in designing the materials with desired properties such as high cation mobility at *rt* in solid-state electrolytes. We hope that this review clarifies the existing relation between different hydroborates poly-anions and the resulting crystal structures, sustaining the material science community in designing novel hydroborate-based compounds.

Supplementary Materials: The following are available online at http://www.mdpi.com/2624-8549/2/4/53/s1, Figure S1: Cation coordination in single metal hydroborates as a function of cation/anion radius ratio C/A. Figure S2: Analogy between temperature polymorphs of $Li_2B_{12}H_{12}$ and C60, and between $Na_2B_{12}H_{12}$ and Ag2S.

Author Contributions: Conceptualization, R.Č.; writing—original draft preparation, R.Č., M.B. and F.M.; writing—review and editing, R.Č., M.B. and F.M.; All authors have read and agreed to the published version of the manuscript.

Funding: This research received no external funding and it was funded by the University of Geneva.

Acknowledgments: We acknowledge all colleagues who shared with us their unpublished results, i.e., the references marked "in preparation".

Conflicts of Interest: The authors declare no conflict of interest.

References and Note

1. Adams, R.M. Nomenclature of inorganic boron compounds. *Pure Appl. Chem.* **1972**, *30*, 681–710. [CrossRef]
2. Lipscomb, W.N. *Boron Hydrides*; W.A. Benjamin Inc.: New York, NY, USA, 1963.
3. Wade, K. The structural significance of the number of skeletal bonding electron-pairs in carboranes, the higher boranes and borane anions, and various transition-metal carbonyl cluster compounds. *J. Chem. Soc. D* **1971**, 792–793. [CrossRef]
4. Mingos, D.M.P. A General Theory for Cluster and Ring Compounds of the Main Group and Transition Elements. *Nat. Phys. Sci.* **1972**, *236*, 99–102. [CrossRef]
5. Clark, J.D. *Ignition!: An Informal History of Liquid Rocket Propellants*; Rutgers University Press: New Brunswick, NJ, USA, 1972.
6. Brown, H.C. *Hydroboration*; W.A. Benjamin Inc.: New York, NY, USA, 1962.
7. Douvris, C.; Ozerov, O.V. Hydrodefluorination of Perfluoroalkyl Groups Using Silylium-Carborane Catalysts. *Science* **2008**, *321*, 1188–1190. [CrossRef] [PubMed]
8. Shao, B.; Bagdasarian, A.L.; Popov, S.; Nelson, H.M. Arylation of Hydrocarbons Enabled by Organosilicon Reagents and Weakly Coordinating Anions. *Science* **2017**, *355*, 1403–1407. [CrossRef]
9. Barfh, R.F.; Soloway, A.H.; Fairchild, R.G.; Brugger, R.M. Boron Neutron Capture Therapy for Cancer. Realities and Prospects. *Cancer* **1992**, *70*, 2995–3007. [CrossRef]
10. Bondarev, O.; Khan, A.A.; Tu, X.; Sevryugina, Y.V.; Jalisatgi, S.S.; Hawthorne, M.F. Synthesis of [closo-$B_{12}(OH)_{11}NH_3$]$^-$: A New Heterobifunctional Dodecaborane Scaffold for Drug Delivery Applications. *J. Am. Chem. Soc.* **2013**, *135*, 13204–13211. [CrossRef]
11. Goswami, L.N.; Ma, L.; Chakravarty, S.; Cai, Q.; Jalisatgi, S.S.; Hawthorne, M.F. Discrete Nanomolecular Polyhedral Borane Scaffold Supporting Multiple Gadolinium(III) Complexes as a High Performance MRI Contrast Agent. *Inorg. Chem.* **2013**, *52*, 1694–1700. [CrossRef]
12. Johnson, J.W.; Brody, J.F. Lithium Closoborane Electrolytes: III. Preparation and Characterization. *J. Electrochem. Soc.* **1982**, *129*, 2213–2219. [CrossRef]
13. Udovic, T.J.; Matsuo, M.; Unemoto, A.; Verdal, N.; Stavila, V.; Skripov, A.V.; Rush, J.J.; Takamura, H.; Orimo, S. Sodium superionic conduction in $Na_2B_{12}H_{12}$. *Chem. Commun.* **2014**, *50*, 3750–3752. [CrossRef]
14. Udovic, T.J.; Matsuo, M.; Tang, W.S.; Wu, H.; Stavila, V.; Soloninin, A.V.; Skoryunov, R.V.; Babanova, O.A.; Skripov, A.V.; Rush, J.J.; et al. Exceptional Superionic Conductivity in Disordered Sodium Decahydro-closo-decaborate. *Adv. Mater.* **2014**, *26*, 7622–7626. [CrossRef] [PubMed]
15. Černý, R.; Schouwink, P. The crystal chemistry of inorganic metal borohydrides and their relation to metal oxides. *Acta Crystallogr. Sect. B Struct. Sci. Cryst. Eng. Mater.* **2015**, *71*, 619–640. [CrossRef] [PubMed]
16. Pauling, L. The Principles Determining the Structure of Complex Ionic Crystals. *J. Am. Chem. Soc.* **1929**, *51*, 1010–1026. [CrossRef]
17. Larsen, P.M.; Schmidt, S.; Schiøtz, J. Robust structural identification via polyhedral template matching. *Model. Simul. Mater. Sci. Eng.* **2016**, *24*, 055007. [CrossRef]
18. Brighi, M.; Murgia, F.; Černý, R. *Closo*-hydroborate sodium salts: An emerging class of room-temperature solid electrolytes. *Cell Rep. Phys. Sci.* **2020**, *1*, 100217d.
19. Kweon, K.E.; Varley, J.B.; Shea, P.; Adelstein, N.; Mehta, P.; Heo, T.W.; Udovic, T.J.; Stavila, V.; Wood, B.C. Structural, Chemical, and Dynamical Frustration: Origins of Superionic Conductivity in closo-Borate Solid Electrolytes. *Chem. Mater.* **2017**, *29*, 9142–9153. [CrossRef]
20. Bradley, J.N.; Green, P.D. Relationship of structure and ionic mobility in solid MAg_4I_5. *Trans. Faraday Soc.* **1967**, *63*, 2516–2521. [CrossRef]
21. Sadikin, Y.; Schouwink, P.; Brighi, M.; Łodziana, Z.; Černý, R. Modified Anion Packing of $Na_2B_{12}H_{12}$ in Close to Room Temperature Superionic Conductors. *Inorg. Chem.* **2017**, *56*, 5006–5016. [CrossRef]
22. Brighi, M.; Murgia, F.; Łodziana, Z.; Schouwink, P.; Wolczyk, A.; Černý, R. A mixed anion borane/carborane as a room temperature Na-ion solid electrolyte. *J. Power Sour.* **2018**, *404*, 7–12. [CrossRef]

23. Sadikin, Y.; Brighi, M.; Schouwink, P.; Černý, R. Superionic Conduction of Sodium and Lithium in Anion-Mixed Hydroborates $Na_3BH_4B_{12}H_{12}$ and $(Li_{0.7}Na_{0.3})_3BH_4B_{12}H_{12}$. *Adv. Energy Mater.* **2015**, *5*, 1501016. [CrossRef]
24. Hansen, B.R.S.; Tumanov, N.; Santoru, A.; Pistidda, C.; Bednarcik, J.; Klassen, T.; Dornheim, M.; Filinchuk, Y.; Jensen, T.R. Synthesis, structures and thermal decomposition of ammine $M_xB_{12}H_{12}$ complexes (M = Li, Na, Ca). *Dalton Trans.* **2017**, *46*, 7770–7781. [CrossRef] [PubMed]
25. Jørgensen, M.; Hansen, B.R.S.; Lee, Y.-S.; Cho, Y.-W.; Jensen, T.R. Crystal Structures and Energy Storage Properties of Ammine Sodium Decahydro-closo-decaboranes ($Na_2B_{10}H_{10}{\cdot}nNH_3$, n = 1,2). *J. Phys. Chem. C* **2019**, *123*, 20160–20166. [CrossRef]
26. Shannon, R.D. Revised effective ionic radii and systematic studies of interatomic distances in halides and chalcogenides. *Acta Crystallogr. Sect. A Cryst. Phys. Diffr. Theor. Gen. Crystallogr.* **1976**, *32*, 751–767. [CrossRef]
27. Hansen, B.R.S.; Paskevicius, M.; Li, H.W.; Akiba, E.; Jensen, T.R. Metal boranes: Progress and applications. *Coord. Chem. Rev.* **2016**, *323*, 60–70. [CrossRef]
28. George, J.; Waroquiers, D.; Di Stefano, D.; Petretto, G.; Rignanese, G.-M.; Hautier, G. The Limited Predictive Power of the Pauling Rules. *Angew. Chem. Int. Ed.* **2020**, *59*, 7569–7575. [CrossRef]
29. Wu, H.; Tang, W.S.; Stavila, V.; Zhou, W.; Rush, J.J.; Udovic, T.J. Structural Behavior of $Li_2B_{10}H_{10}$. *J. Phys. Chem. C* **2015**, *119*, 6481–6487. [CrossRef]
30. Verdal, N.; Her, J.-H.; Stavila, V.; Soloninin, A.V.; Babanova, O.A.; Skripov, A.V.; Udovic, T.J.; Rush, J.J. Complex high-temperature phase transitions in $Li_2B_{12}H_{12}$ and $Na_2B_{12}H_{12}$. *J. Solid State Chem.* **2014**, *212*, 81–91. [CrossRef]
31. Hansen, B.R.S.; Paskevicius, M.; Jørgensen, M.; Jensen, T.R. Halogenated Sodium-closo-Dodecaboranes as Solid-State Ion Conductors. *Chem. Mater.* **2017**, *29*, 3423–3430. [CrossRef]
32. Skripov, A.V.; Soloninin, A.V.; Babanova, O.A.; Skoryunov, R.V. Nuclear Magnetic Resonance Studies of Atomic Motion in Borohydride-Based Materials: Fast Anion Reorientations and Cation Diffusion. *J. Alloys Compd.* **2015**, *645*, S428–S433. [CrossRef]
33. Varley, J.B.; Kweon, K.; Mehta, P.; Shea, P.; Heo, T.W.; Udovic, T.J.; Stavila, V.; Wood, B.C. Understanding Ionic Conductivity Trends in Polyborane Solid Electrolytes from Ab Initio Molecular Dynamics. *ACS Energy Lett.* **2017**, *2*, 250–255. [CrossRef]
34. Skripov, A.V.; Soloninin, A.V.; Babanova, O.A.; Skoryunov, R.V. Anion and Cation Dynamics in Polyhydroborate Salts: NMR Studies. *Molecules* **2020**, *25*, 2940. [CrossRef]
35. Verdal, N.; Udovic, T.J.; Stavila, V.; Tang, W.S.; Rush, J.J.; Skripov, A.V. Anion Reorientations in the Superionic Conducting Phase of $Na_2B_{12}H_{12}$. *J. Phys. Chem. C* **2014**, *118*, 17483–17489. [CrossRef]
36. Callear, S.K.; Nickels, E.A.; Jones, M.O.; Matauo, M.; Orimo, S.-I.; Edwards, P.; David, W.I.F. Order and disorder in lithium tetrahydroborate. *J. Mater. Sci.* **2011**, *46*, 566–569. [CrossRef]
37. Heere, M.; Hansen, A.L.; Payandeh, S.H.; Aslan, N.; Gizer, G.; Sørby, M.H.; Hauback, B.C.; Ristidda, C.; Dornheim, M.; Lohstroh, W. Dynamics of porous and amorphous magnesium borohydride to understand solid state Mg-ionconductors. *Sci. Rep.* **2020**, *10*, 9080. [CrossRef] [PubMed]
38. Tiritiris, I.; Schleid, T.; Müller, K. Solid-State NMR Studies on Ionic *closo*-Dodecaborates. *Appl. Magn. Reson.* **2007**, *32*, 459–481. [CrossRef]
39. Verdal, N.; Udovic, T.J.; Rush, J.J.; Cappelletti, R.L.; Zhou, W. Reorientational Dynamics of the Dodecahydro-closo-dodecaborate Anion in $Cs_2B_{12}H_{12}$. *J. Phys. Chem. A* **2011**, *115*, 2933–2938. [CrossRef]
40. Skripov, A.V.; Babanova, O.A.; Soloninin, A.V.; Stavila, V.; Verdal, N.; Udovic, T.J.; Rush, J.J. Nuclear Magnetic Resonance Study of Atomic Motion in $A_2B_{12}H_{12}$ (A = Na, K, Rb, Cs): Anion Reorientations and Na^+ Mobility. *J. Phys. Chem. C* **2013**, *117*, 25961–25968. [CrossRef]
41. Bürgi, H.B.; Restori, R.; Schwarzenbach, D. Structure of C60: Partial orientational order in the room-temperature modification of C60. *Acta Crystallogr. Sect. B Struct. Sci. Cryst. Eng. Mater.* **1993**, *49*, 832–838. [CrossRef]
42. Williams, R.E. The polyborane, carborane, carbocation continuum: Architectural patterns. *Chem. Rev.* **1992**, *92*, 177–207. [CrossRef]
43. Aihara, J. Three-dimensional aromaticity of polyhedral boranes. *J. Am. Chem. Soc.* **1978**, *100*, 3339–3342. [CrossRef]
44. Von Ragué Schleyer, P.; Najafian, K. Stability and Three-Dimensional Aromaticity of *closo*-Monocarbaborane Anions, $CB_{n-1}H_n^-$, and *closo*-Dicarboranes, $C_2B_{n-2}H_n$. *Inorg. Chem.* **1998**, *37*, 3454–3470. [CrossRef] [PubMed]

45. Douvris, C.; Michl, J. Update 1 of: Chemistry of the Carba-*closo*-dodecaborate(−) Anion, $CB_{11}H_{12}^-$. *Chem. Rev.* **2013**, *113*, PR179–PR233. [CrossRef] [PubMed]
46. Hofmann, M.; Fox, M.A.; Greatrex, R.; von Ragué Schleyer, P.; Williams, R.E. Empirical and ab Initio Energy/Architectural Patterns for 73 nido-6⟨V⟩-Carborane Isomers, from $B_6H_9^-$ to $C_4B_2H_6$. *Inorg. Chem.* **2001**, *40*, 1790–1801. [CrossRef] [PubMed]
47. Payandeh, S.H.; Asakura, R.; Avramidou, P.; Rentsch, D.; Łodziana, Z.; Černý, R.; Remhof, A.; Battaglia, C. Nido-Borate/Closo-Borate Mixed-Anion Electrolytes for All-Solid-State Batteries. *Chem. Mater.* **2020**, *32*, 1101–1110.
48. Tang, W.S.; Matsuo, M.; Wu, H.; Stavila, V.; Zhou, W.; Talin, A.A.; Soloninin, A.V.; Skoryunov, R.V.; Babanova, O.A.; Skripov, A.V.; et al. Liquid-Like Ionic Conduction in Solid Lithium and Sodium Monocarba—closo—Decaborates Near or at Room Temperature. *Adv. Energy Mater.* **2016**, *6*, 1502237. [CrossRef]
49. Bergerhoff, G.; Brown, I.D.; Allen, F. *Crystallographic Databases*; (Hrsg.) International Union of Crystallography: Chester, UK, 1987. Available online: http://www.fiz-karlsruhe.de/icsd_home.html.
50. Villars, P.; Cenzual, K. *Pearson's Crystal Data-Crystal Structure Database for Inorganic Compounds*; ASM International Materials Park: Russel Township, OH, USA, 2015.
51. Villars, P.; Cenzual, K.; Gladyshevskii, R.; Iwata, S. Pauling File—Towards a holistic view. *Chem. Met. Alloys* **2018**, *11*, 43–76. [CrossRef]
52. Paskevicius, M.; Jepsen, L.H.; Schouwink, P.; Černý, R.; Ravnsbaeck, D.; Filinchuk, Y.; Dornheim, M.; Besenbacher, F.; Jensen, T.R. Metal borohydrides and derivatives—Synthesis, structure and properties. *Chem. Soc. Rev.* **2017**, *46*, 1565–1634. [CrossRef]
53. Axtell, J.C.; Saleh, L.M.A.; Qian, E.A.; Wixtrom, A.I.; Spokoyny, A.M. Synthesis and Applications of Perfunctionalized Boron Clusters. *Inorg. Chem.* **2018**, *57*, 2333–2350. [CrossRef]
54. Muetterties, E.L.; Balthis, J.H.; Chia, Y.T.; Knoth, W.H.; Miller, H.C. Chemistry of Boranes. VIII. Salts and Acids of $B_{10}H_{10}^{-2}$ and $B_{12}H_{12}^{-2}$. *Inorg. Chem.* **1964**, *3*, 444–451. [CrossRef]
55. Sivaev, I.B.; Prikaznov, A.V.; Naoufal, D. Fifty years of the closo-decaborate anion chemistry. *Collect. Czechoslov. Chem. Commun.* **2010**, *75*, 1149–1199. [CrossRef]
56. Sivaev, I.B.; Bregadze, V.I.; Sjöberg, S. Chemistry of closo-Dodecaborate Anion $[B_{12}H_{12}]^{2-}$: A Review. *Collect. Czechoslov. Chem. Commun.* **2002**, *67*, 679–727. [CrossRef]
57. Housecroft, C.E. Carboranes as guests, counterions and linkers in coordination polymers and networks. *J. Organomet. Chem.* **2015**, *798*, 218–228. [CrossRef]
58. Malinina, E.A.; Avdeeva, V.V.; Goeva, L.V.; Kuznetsov, N.T. Coordination Compounds of Electron-Deficient Boron Cluster Anions $B_nH_n^{2-}$ (n = 6, 10, 12). *Russ. J. Inorg. Chem.* **2010**, *55*, 2148–2202. [CrossRef]
59. Müller, U. *Symmetry Relationships between Crystal Structures*; Oxford University Press: Oxford, UK, 2013.
60. Blatov, V.A. Multipurpose christalochemical analysis with the program package TOPOS. *IUCr Comp. Comm. Newsl.* **2006**, *7*, 4–38.
61. Topospro. Available online: https://topospro.com/databases/ttd/ (accessed on 29 September 2020).
62. Her, J.-H.; Yousufuddin, M.; Zhou, W.; Jalisatgi, S.S.; Kulleck, J.G.; Zan, J.A.; Hwang, S.-J.; Bowman, R.C.; Udovic, T.J. Crystal structure of $Li_2B_{12}H_{12}$: A possible intermediate species in the decomposition of $LiBH_4$. *Inorg. Chem.* **2008**, *47*, 9757–9759. [CrossRef]
63. Paskevicius, M.; Pitt, M.P.; Brown, D.H.; Sheppard, D.A.; Chumphongphan, S.; Buckley, C.E. First-order phase transition in the $Li_2B_{12}H_{12}$ system. *Phys. Chem. Chem. Phys.* **2013**, *15*, 15825–15828. [CrossRef]
64. This work. The symmetry of *Pa*-3 from ref. [63] was corrected to *Fm*-3.
65. Tang, W.S.; Unemoto, A.; Zhou, W.; Stavila, V.; Matsuo, M.; Wu, H.; Orimo, S.-I.; Udovic, T.J. Unparalleled lithium and sodium superionic conduction in solid electrolytes with large monovalent cage-like anions. *Energy Environ. Sci.* **2015**, *8*, 3637–3645. [CrossRef]
66. Jørgensen, M.; Shea, P.T.; Tomich, A.; Varley, J.B.; Bercx, M.; Lovera, S.; Černý, R.; Zhou, W.; Udovic, T.J.; Lavallo, V.; et al. Understanding Superionic Conductivity in Lithium and Sodium Salts of Weakly Coordinating *Closo*-Hexahalocarbaborate Anions. *Chem. Mater.* **2020**, *32*, 1475–1487. [CrossRef]
67. Payandeh, S.H.; Rentsch, D.; Asakura, R.; Łodziana, Z.; Bigler, L.; Černý, R.; Remhof, A.; Battaglia, C. Nido-Hydroborate based Electrolytes for All-Solid-State Lithium Batteries. 2020; in preparation.

68. Tang, W.S.; Yoshida, K.; Soloninin, A.V.; Skoryunov, R.V.; Babanova, O.A.; Skripov, A.V.; Dimitrievska, M.; Stavila, V.; Orimo, S.-I.; Udovic, T.J. Stabilizing Superionic-Conducting Structures via Mixed-Anion Solid Solutions of Monocarba-closo-borate Salts. *ACS Energy Lett.* **2016**, *1*, 659–664. [CrossRef]
69. Moury, R.; Łodziana, Z.; Remhof, A.; Duchêne, L.; Roedern, E.; Gigante, A.; Hagemann, H. Pressure-induced phase transitions in $Na_2B_{12}H_{12}$, structural investigation on a candidate for solid-state electrolyte. *Acta Crystallogr. Sect. B Struct. Sci. Cryst. Eng. Mater.* **2019**, *75*, 406–413. [CrossRef]
70. Wu, H.; Tang, W.S.; Zhou, W.; Stavila, V.; Rush, J.J.; Udovic, T.J. The structure of monoclinic $Na_2B_{10}H_{10}$: A combined diffraction, spectroscopy, and theoretical approach. *CrystEngComm* **2015**, *17*, 3533–3540. [CrossRef]
71. Dunbar, A.C.; Macor, J.A.; Girolami, G.S. Synthesis and single crystal structure of sodium octahydrotriborate, NaB_3H_8. *Inorg. Chem.* **2014**, *53*, 822–826. [CrossRef] [PubMed]
72. Wu, H.; Tang, W.S.; Zhou, W.; Tarver, J.D.; Stavila, V.; Brown, C.M.; Udovic, T.J. The low-temperature structural behavior of sodium 1-carba-closo-decaborate: $NaCB_9H_{10}$. *J. Solid State Chem.* **2016**, *243*, 162–167. [CrossRef]
73. Tang, W.S.; Dimitrievska, M.; Stavila, V.; Zhou, W.; Wu, H.; Talin, A.A.; Udovic, T.J. Order−Disorder Transitions and Superionic Conductivity in the Sodium nido—Undeca(carba)borates. *Chem. Mater.* **2017**, *29*, 10496–10509. [CrossRef]
74. Yoshida, K.; Sato, T.; Unemoto, A.; Matsuo, M.; Ikeshoji, T.; Udovic, T.J.; Orimo, S.-I. Fast sodium ionic conduction in $Na_2B_{10}H_{10}$-$Na_2B_{12}H_{12}$ pseudo-binary complex hydride and application to a bulk-type all-solid-state battery. *Appl. Phys. Lett.* **2017**, *110*, 103901. [CrossRef]
75. Duchêne, L.; Kuhnel, R.S.; Rentsch, D.; Remhof, A.; Hagemann, H.; Battaglia, C. A highly stable sodium solid-state electrolyte based on a dodeca/deca-borate equimolar mixture. *Chem. Commun.* **2017**, *53*, 4195–4198. [CrossRef] [PubMed]
76. Wunderlich, J.A.; Lipscomb, W.N. Structure of $B_{12}H_{12}^{-2}$ ion. *J. Am. Chem. Soc.* **1960**, *82*, 4427–4428. [CrossRef]
77. Hofmann, K.; Albert, B. Crystal structures of $M_2[B_{10}H_{10}]$ (M = Na, K, Rb) via real space simulated annealing powder techniques. *Z. Kristall.* **2005**, *220*, 142–146. [CrossRef]
78. Grinderslev, J.B.; Møller, K.T.; Yan, Y.; Chen, X.-M.; Li, Y.; Li, H.-W.; Zhou, W.; Skibsted, J.; Chen, X.; Jensen, T.R. Potassium octahydridotriborate: Diverse polymorphism in a potential hydrogen storage material and potassium ion conductor. *Dalton Trans.* **2019**, *48*, 8872–8881. [CrossRef]
79. Kuznetsov, I.Y.; Vinitskii, D.M.; Solntsev, K.A.; Kuznetsov, N.T. The Crystal Structure of $K_2B_6H_6$ and $Cs_2B_6H_6$. *Russ. J. Inorg. Chem.* **1987**, *32*, 1803–1804.
80. Dimitrievska, M.; Wu, H.; Stavila, V.; Babanova, O.A.; Skoryunov, R.V.; Soloninin, A.V.; Zhou, W.; Trump, B.A.; Andersson, M.S.; Skripov, A.V.; et al. Structural and Dynamical Properties of Potassium Dodecahydro-monocarba-closo-dodecaborate: $KCB_{11}H_{12}$. *J. Phys. Chem. C* **2020**, *124*, 17992–18002. [CrossRef]
81. Bernhardt, E.; Brauer, D.; Finze, M.; Willner, H. Closo-$[B_{21}H_{18}]^-$: A Face-Fused Diicosahedral Borate Ion. *Angew. Chem. Int. Ed.* **2007**, *46*, 2927–2930. [CrossRef] [PubMed]
82. Sadikin, Y.; Skoryunov, R.V.; Babanova, O.A.; Soloninin, A.V.; Lodziana, Z.; Brighi, M.; Skripov, A.V.; Černý, R. Anion disorder in $K_3BH_4B_{12}H_{12}$ and its effect on cation mobility. *J. Phys. Chem. C* **2017**, *121*, 5503–5514. [CrossRef]
83. Tiritiris, I.; Schleid, T. The Dodecahydro-*closo*-Dodecaborates $M_2[B_{12}H_{12}]$ of the Heavy Alkali Metals (M = K^+, Rb+, NH_4^+, Cs^+) and their Formal Iodide Adducts $M_3I[B_{12}H_{12}]$ (= $MI{\cdot}M_2[B_{12}H_{12}]$). *Z. Anorg. Allg. Chem.* **2003**, *629*, 1390–1402. [CrossRef]
84. Dimitrievska, M.; Stavila, V.; Soloninin, A.V.; Skoryunov, R.V.; Babanova, O.A.; Wu, H.; Zhou, W.; Tang, W.S.; Faraone, A.; Tarver, J.D.; et al. Nature of Decahydro-Closo-Decaborate Anion Reorientations in an Ordered Alkali-Metal Salt: $Rb_2B_{10}H_{10}$. *J. Phys. Chem. C* **2018**, *122*, 15198–15207. [CrossRef]
85. Guggenberger, L.J. Chemistry of boranes. XXXIII. The crystal structure of $Rb_2B_9H_9$. *Inorg. Chem.* **1968**, *7*, 2260–2264. [CrossRef]
86. DeBoer, B.G.; Zalkin, A.; Templeton, D.H. The crystal structure of the rubidium salt of an octa-decahydroeicosaborate(2-) photoisomer. *Inorg. Chem.* **1968**, *7*, 1085–1090. [CrossRef]
87. Schouwink, P.; Sadikin, Y.; van Beek, W.; Černý, R. Experimental observation of polymerization from BH_4 to $B_{12}H_{12}$ in mixed-anion $A_3BH_4B_{12}H_{12}$ (A = Rb, Cs). *Int. J. Hydrogen Energy* **2015**, *40*, 10902–10907. [CrossRef]
88. Tiritiris, I.; Schleid, T.; Müuller, K.; Preetz, W. Structural Investigations on $Cs_2[B_{12}H_{12}]$. *Z. Anorg. Allg. Chem.* **2000**, *626*, 323–325. [CrossRef]

89. Verdal, N.; Wu, H.; Udovic, T.J.; Stavila, V.; Zhou, W.; Rush, J.J. Evidence of a transition to reorientational disorder in the cubic alkali-metal dodecahydro-closo-dodecaborates. *J. Solid State Chem.* **2011**, *184*, 3110–3116. [CrossRef]
90. Deiseroth, H.J.; Sommer, O.; Binder, H.; Wolfer, K.; Frei, B. CsB_3H_8: Crystal Structure and Upgrading of the Synthesis. *Z. Anorg. Allg. Chem.* **1989**, *571*, 21–28. [CrossRef]
91. Schlüter, F.; Bernhardt, E. Syntheses and Crystal Structures of the *closo*-Borate $M[B_8H_9]$ (M = $[PPh_4]^+$ and $[N(n\text{-}Bu_4)]^+$). *Inorg. Chem.* **2012**, *51*, 511–517. [CrossRef] [PubMed]
92. Greenwood, N.N.; McGinnety, J.A.; Owen, J.D. Crystal structure of caesium tetradecahydrononaborate(1–), CsB_9H_{14}. *J. Chem. Soc. Dalton Trans.* **1972**, 986–989. [CrossRef]
93. Schlüter, F.; Bernhardt, E. Fluorination of *closo*-$[B_{21}H_{18}]^-$ with *a*HF and F_2 to yield *closo*-$[B_{21}H_{18-x}F_x]^-$ (x = 1–3) and *closo*-$[B_{21}F_{18}]^-$. *Z. Anorg. Allg. Chem.* **2012**, *638*, 594–601. [CrossRef]
94. Černý, R.; Brighi, M.; Dimitrievska, M.; Udovic, T.J. Dodeca-carbahydroborates of Caesium and Rubidium, crystal structure and anions dynamic. 2020; in preparation.
95. Franken, A.; Bullen, N.J.; Jelínek, T.; Thornton-Pett, M.; Teat, S.J.; Clegg, W.; Kennedy, J.D.; Hardie, M.J. Structural chemistry of halogenated monocarbaboranes: The extended structures of Cs[1-$HCB_9H_4Br_5$], Cs[1-$HCB_{11}H_5Cl_6$] and Cs[1-$HCB_{11}H_5Br_6$]. *New J. Chem.* **2004**, *28*, 1499–1505. [CrossRef]
96. Jelínek, T.; Baldwin, P.; Scheldt, W.R.; Reed, C.A. New Weakly Coordinating Anions. 2. Derivatization of the Carborane Anion $CB_{11}H_{12}^-$. *Inorg. Chem.* **1993**, *32*, 1982–1990. [CrossRef]
97. Rius, J.; Romerosa, A.; Teixidor, F.; Casabo, J.; Miravitlles, C. Phase transitions in cesium 7,8-dicarbaundecaborate(12): A new one-dimensional cesium solid electrolyte at 210 °C. *Inorg. Chem.* **1991**, *30*, 1376–1379. [CrossRef]
98. Tiritiris, I. Untersuchungen zu Reaktivität, Aufbau und Struktureller Dynamik von Salzartigen Closo Dodekaboraten. Ph.D. Thesis, Universität Stuttgart Fakultät Chemie, Stuttgart, Germany, 2003.
99. Calabrese, J.C.; Gaines, D.F.; Hildebrandt, S.J.; Morris, J.H. The Low Temperature Crystal and Molecular Structure of Beryllium Bis(octahydrotriborate), $Be(B_3H_8)_2$. *J. Am. Chem. Soc.* **1976**, *98*, 5489–5492. [CrossRef]
100. Gaines, D.F.; Walsh, J.L.; Calabrese, J.C. Low-Temperature Crystal and Molecular Structures of 2-Tetrahydroborato-2- berylla-nido-hexaborane(11) and 2,2′-*commo*-Bis[2-berylla-nido-hexaborane1(1)]. *Inorg. Chem.* **1978**, *17*, 1242–1248. [CrossRef]
101. Stavila, V.; Her, J.H.; Zhou, W.; Hwang, S.J.; Kim, C.; Ottley, L.A.M.; Udovic, T.J. Probing the structure, stability and hydrogen storage properties of calcium dodecahydro-*closo*-dodecaborate. *J. Solid State Chem.* **2010**, *183*, 1133–1140. [CrossRef]
102. Jørgensen, M.; Zhou, W.; Wu, H.; Udovic, T.J.; Jensen, T.R.; Paskevicius, M.; Černý, R. Polymorphism of CaB10H10 and Its Hydrates. 2020; in preparation.
103. Her, J.H.; Wu, H.; Verdal, N.; Zhou, W.; Stavila, V.; Udovic, T.J. Structures of the strontium and barium dodecahydro-*closo*-dodecaborates. *J. Alloys Compd.* **2012**, *514*, 71–75. [CrossRef]
104. Goedde, D.M.; Windler, G.K.; Girolami, G.S. Synthesis and Characterization of the Homoleptic Octahydrotriborate Complex $Cr(B_3H_8)_2$ and Its Lewis Base Adducts. *Inorg. Chem.* **2007**, *46*, 2814–2823. [CrossRef] [PubMed]
105. Didelot, E.; Łodziana, Z.; Murgia, F.; Černý, R. Ethanol—and methanol—Coordinated and solvent—free dodecahydro closo-dodecaborates of 3d transition metals and of magnesium. *Crystals* **2019**, *9*, 372. [CrossRef]
106. Didelot, E.; Sadikin, Y.; Łodziana, Z.; Černý, R. Hydrated and anhydrous dodecahydro closo-dodecaborates of 3d transition metals and of magnesium. *Solid State Sci.* **2019**, *90*, 86–94. [CrossRef]
107. Sadikin, Y.; Didelot, E.; Łodziana, Z.; Černý, R. Synthesis and crystal structure of solvent-free dodecahydro *closo*-dodecaborate of nickel, $NiB_{12}H_{12}$. *Dalton Trans.* **2018**, *47*, 5843–5849. [CrossRef]
108. Paskevicius, M.; Hansen, B.R.S.; Jørgensen, M.; Richter, B.; Jensen, T.R. Multifunctionality of Silver *closo*-Boranes. *Nat. Commun.* **2017**, *8*, 15136. [CrossRef]
109. Xie, Z.; Jelinek, T.; Bau, R.; Reed, C.A. New weakly coordinating anions. 3. Useful silver and trityl salt reagents of carborane anions. *J. Am. Chem. Soc.* **1994**, *116*, 1907–1913. [CrossRef]
110. Xie, Z.; Wu, B.; Mak, T.C.W.; Reed, C.A. Structural Diversity in Silver Salts of Hexahalogenocarborane Anions, $Ag(CB_{11}H_6X_6)$ (X = Cl, Br or I). *J. Chem. Soc. Dalton Trans.* **1997**, *640*, 1213–1217. [CrossRef]
111. Nguyen-Duc, V. New Salt-Like Dodecahydro-Closo-Dodecaborates and Efforts for the Partial Hydroxylation of $[B_{12}H_{12}]^{2-}$ Anions. Ph.D. Thesis, Universität Stuttgart Fakultät Chemie, Stuttgart, Germany, 2009.

112. Tiritiris, I.; Van, N.D.; Schleid, T. Two Dodecahydro-*closo*-Dodecaborates with *Lone-Pair* Cations of the 6th Period in Comparison: $Tl_2[B_{12}H_{12}]$ and $Pb(H_2O)_3[B_{12}H_{12}]\cdot 3H_2O$. *Z. Anorg. Allg. Chem.* **2011**, *637*, 682–688. [CrossRef]
113. Kleeberg, F.M.; Zimmermann, L.W.; Schleid, T. Synthesis and Crystal Structure of anhydrous $Pb_2[B_{12}H_{12}]$. *Z. Anorg. Allg. Chem.* **2014**, *640*, 2352.
114. Tang, W.S.; Udovic, T.J.; Stavila, V. Altering the structural properties of $A_2B_{12}H_{12}$ compounds via cation and anion modifications. *J. Alloys Compd.* **2015**, *645*, S200–S204. [CrossRef]
115. He, L.Q.; Li, H.W.; Nakajima, H.; Tumanov, N.; Filinchuk, Y.; Hwang, S.J.; Sharma, M.; Hagemann, H.; Akiba, E. Synthesis of a Bimetallic Dodecaborate $LiNaB_{12}H_{12}$ with Outstanding Superionic Conductivity. *Chem. Mater.* **2015**, *27*, 5483–5486. [CrossRef]
116. Tumanov, N.; He, L.; Sadikin, Y.; Brighi, M.; Li, H.W.; Akiba, E.; Černý, R.; Filinchuk, Y. Structural study of a bimetallic dodecaborate LiKB12H12 synthesized from decaborane B10H14. in preparation.
117. Polyakova, I.N.; Malinina, E.A.; Kuznetsov, N.T. Crystal Structures of Cesium and Dimethylammonium Cupradecaborates, $Cs[CuB_{10}H_{10}]$ and $(CH_3)_2NH_2[CuB_{10}H_{10}]$. *Crystallogr. Rep.* **2003**, *48*, 84–91. [CrossRef]
118. Malinina, E.A.; Zhizhin, K.Y.; Polyakova, I.N.; Lisovskii, M.V.; Kuznetsov, N.T. Silver(I) and Copper(I) Complexes with the closo-Decaborate Anion $B_{10}H_{10}^{-}$ as a Ligand. *Russ. J. Inorg. Chem.* **2002**, *47*, 1158–1167.
119. Yisgedu, T.B.; Huang, Z.; Chen, X.; Lingam, H.K.; King, G.; Highley, A.; Maharrey, S.; Woodward, P.M.; Behrens, R.; Shore, S.G.; et al. The structural characterization of $(NH_4)_2B_{10}H_{10}$ and thermal decomposition studies of $(NH_4)_2B_{10}H_{10}$ and $(NH_4)_2B_{12}H_{12}$. *Int. J. Hydrogen Energy* **2012**, *37*, 4267–4273. [CrossRef]
120. Huang, Z.; Chen, X.; Yisgedu, T.; Meyers, E.A.; Shore, S.G.; Zhao, J.C. Ammonium Octahydrotriborate ($NH_4B_3H_8$): New Synthesis, Structure, and Hydrolytic Hydrogen Release. *Inorg. Chem.* **2011**, *50*, 3738–3742. [CrossRef]
121. Derdziuk, J.; Malinowski, P.J.; Jaron, T. The synthesis, structural characterization and thermal decomposition studies of $(N_2H_5)_2B_{12}H_{12}$ and its solvates. *Int. J. Hydrogen Energy* **2019**, *44*, 27030–27038. [CrossRef]
122. Schlüter, F.; Bernhardt, E. Syntheses and Crystal Structures of the closo-Borates $M_2[B_7H_7]$ and $M[B_7H_8]$ ($M = PPh_4$, PNP, and $N(n\text{-}Bu_4)$): The Missing Crystal Structure in the Series $[B_nH_n]_2$- (n = 6–12). *Inorg. Chem.* **2011**, *50*, 2580–2589. [CrossRef]
123. McGrath, T.D.; Welch, A.J. $[Ph_3PH][nido\text{-}B_{11}H_{14}]$. *Acta Crystallogr. Sect. C Struct. Chem.* **1997**, *53*, 229–231. [CrossRef]
124. Polyakova, I.N.; Malinina, E.A.; Drozdova, V.V.; Kuznetsov, N.T. The Isomorphous Substitution of $2H^+$ for the Cu^{2+} Cation in the Complex of Bis(aminoguanidine) copper (II): Crystal Structures of $(Cu_{0.61}H_{0.78}Agu_2)B_{12}H_{12}$ and $(HAgu)_2B_{12}H_{12}$. *Crystallogr. Rep.* **2009**, *54*, 831–836. [CrossRef]